PERGAMON

International Journal of Solids and Structures 40 (2003) 3787–3805

INTERNATIONAL JOURNAL OF SOLIDS and STRUCTURES

www.elsevier.com/locate/ijsolstr

Three-dimensional asymptotic stress field in the vicinity of the circumference of a penny shaped discontinuity

Reaz A. Chaudhuri *

Department of Materials Science and Engineering, University of Utah, Salt lake City, Utah 84112, USA

Received 2 October 2001; received in revised form 25 November 2002

Abstract

An eigenfunction expansion method is presented to obtain three-dimensional asymptotic stress fields in the vicinity of the front of a penny shaped discontinuity, e.g., crack, anticrack (infinitely rigid lamella), etc., subjected to the far-field torsion (mode III), extension/bending (mode I) and sliding shear/twisting (mode II) loadings. Five different discontinuity-surface boundary conditions are considered: (i) penny shaped crack, (ii) penny shaped anticrack or perfectly bonded thin rigid inclusion, (iii) penny shaped thin transversely rigid inclusion (frictionless planar slip permitted), (iv) penny shaped thin rigid inclusion in part perfectly bonded, the remainder with frictionless slip, and (v) penny shaped thin rigid inclusion alongside penny shaped crack. The computed stress singularity for a penny shaped anticrack is the same as that of the corresponding crack. The main difference is, however, that all the stress components at the circular tip of an anticrack depend on Poisson's ratio under modes I and II.

Keywords: Penny shaped crack; Penny shaped rigid inclusion; Anticrack; Hydrogen embrittlement; Three-dimensional; Stress singularity; Asymptotic; Frictionless slip; Mixed boundary condition

1. Introduction

The problem of a thick plate weakened by an embedded penny shaped crack (Fig. 1) has a long history dating back to solutions due to Sack (1946) and Sneddon (1946). Sack (1946) was the first to extend Griffith's (two-dimensional) theory of rupture to a three-dimensional one by considering a penny shaped (circular) crack of radius a, subjected to a stress field acting normal to the plane of the crack. By treating the crack as an oblate spheroid and using Neuber's solution of the equations of equilibrium in oblate spheroidal coordinate system, Sack (1946) was able to derive the critical value of the tensile stress, σ_c, given by

$$\sigma_c = \left[\frac{\pi E \gamma_s}{2(1-\nu^2)a}\right]^{\frac{1}{2}},$$

* Tel.: +1-801-581-6863; fax: +1-801-581-4816.
E-mail address: r.chaudhuri@m.cc.utah.edu (R.A. Chaudhuri).

0020-7683/03/$ - see front matter © 2003 Elsevier Science Ltd. All rights reserved.
doi:10.1016/S0020-7683(03)00017-9

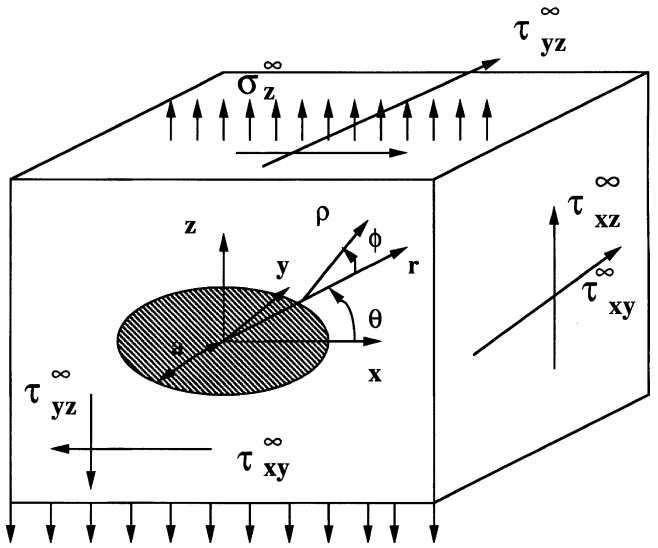

Fig. 1. A penny shaped discontinuity, associated local coordinate system (ρ, ϕ, θ) and far-field loadings.

where E and v are Young's modulus and Poisson's ratio, respectively, and γ_s is the surface energy of the material. Sneddon (1946) solved the same problem using a cylindrical polar coordinate system, r, θ, z, where $r = 0$ represents the crack tip or front, and $z = 0$ denotes the plane of the crack. Sneddon's solution is based on the method of Hankel transform that reduces the problem to a pair of dual integral equations.

A penny shaped rigid inclusion is essentially a penny shaped crack filled with an infinitely rigid lamella (in this case, an embedded thin circular platelet or single crystal layer, or atomic hydrogen layer diffused into metallic lattice or grain boundary), which unlike a crack transmits tractions, but prevents a displacement discontinuity, and has been christened "anticrack" by Dundurs and Markenscoff (1989). Penny shaped rigid inclusions have important applications in the field of materials science, because they are idealized representations of various kinds of high modulus reinforcements (e.g., SiC, $A1_2O_3$, etc. in the form of platelets, etc.), embrittlements (e.g., hydrogen embrittlement (HE)), and are as much a source of materials failure as cracks. Metallic materials have been known to fail at a level much lower than the (plane strain) fracture toughness parameter, K_{IC}, due to cooperative interaction of the applied stress field, and environmentally assisted cracking (EAC) processes, such as HE, stress corrosion cracking (SCC), etc. Various models for HE are discussed in standard texts, e.g., Hertzberg (1996). It is presently believed by materials scientists that molecular hydrogen is dissociated by a chemisorption process on iron, which allows the liberated atomic hydrogen to diffuse internally into the metallic lattice and grain boundary thus forming an embrittled layer. Atomic hydrogen can diffuse rapidly through a metal lattice, because its size is smaller than the lattice parameter. More significantly, hydrogen transport rates in association with dislocation motion can be several orders of magnitude higher than that due to lattice diffusion (Hertzberg, 1996).

Although the two-dimensional analysis pertaining to the asymptotic displacement and stress fields in the vicinity of the tip of a rigid line (plane strain/stress) inclusion has received some attention during the last four decades, e.g., Sih (1965), Atkinson (1973), Brussat and Westman (1974, 1975), Hasebe et al. (1984), Dundurs and Markenscoff (1989), the corresponding three-dimensional analysis of a penny shaped anticrack (infinitely rigid circular lamella) remains, to the author's knowledge, to be addressed in the literature. One of the goals of the present study is to fill this analytical gap.

Admittedly, the Hankel transform combined with the dual integral equations approach due to Sneddon (1946) followed by others is a valuable tool, which can also be employed to solve the penny shaped

anticrack problem. It is, however, not as simple and straightforward as the eigenfunction approach, pioneered by Williams (1952) in two-dimensional analysis of angular corners, and extended to three-dimensional analysis of through cracks and bimaterial interface cracks by Chaudhuri and Xie (2000), and Xie and Chaudhuri (1998), respectively. It is worthwhile to note here that although the Williams (1952) eigenfunction expansion method for solution to the plane stress problem of a plate with a corner dates back to the time when the three-dimensional penny shaped crack problem was first addressed by Sack (1946) and Sneddon (1946), no connection was explored by researchers between the two sets of studies, which is the primary focus in what follows. Finally, although the eigenfunction method has been successfully implemented to compute the orders of three-dimensional stress singularities at the tips of cracks in homogeneous materials (Chaudhuri and Xie, 2000) and bimaterial interface cracks (Xie and Chaudhuri, 1998), it has not been applied to the computation of three-dimensional asymptotic stress field at the circular tip of a penny shaped discontinuity, such as a crack or anticrack, which is the primary objective of the present investigation.

2. Problem formulation

Fig. 1 shows the schematic diagram of an isotropic elastic body weakened by the presence of a penny shaped crack or thin rigid inclusion of radius, a, subjected to general far-field loading, and the attached Cartesian and cylindrical polar coordinate systems, (x, y, z) and (r, θ, z), respectively. The circular tip of the crack or the thin rigid inclusion weakening the elastic body of infinite extent is located at $r = a$, a being the radius, while the mid-plane of the body is located at $z = 0$, the same as the plane of the crack or rigid inclusion.

The key step is the selection of an appropriate local coordinate system (see Fig. 1(a)). A local curvilinear coordinate system (ρ, ϕ, θ) is convenient to describe the local deformation behavior of the afore-mentioned elastic body in the vicinity of the tip of the penny shaped crack or thin rigid inclusion. The components of the displacements in the radial and tangential directions are represented by U_ρ, U_ϕ, while the component in the circumferential or θ-direction is denoted by U_θ.

The local coordinate system is, as mentioned above, comprised of ρ, which denotes the radial direction from a point located on the circular tip of the crack or rigid inclusion, ϕ which denotes the angular direction measured counterclockwise from the plane of the penny shaped crack or thin rigid inclusion, and θ, which is positive counterclockwise (looking from top) along the boundary of the crack or rigid inclusion. Then the covariant and contravariant components of the base and reciprocal base vectors, called the Euclidean metric and associated metric tensors, are derived, which yield the components of the Christoffel three-index symbol of the second kind (Fung, 1965; Green and Zerna, 1968; Korn and Korn, 1968). Finally, the strain–displacement relations and equations of equilibrium in terms of the physical components of the displacement vector are derived below.

The line element in the local curvilinear coordinate system (ρ, ϕ, θ) is given by

$$\mathrm{d}s^2 = \mathrm{d}\rho^2 + \rho^2\mathrm{d}\phi^2 + (a + \rho\cos\phi)^2\mathrm{d}\theta^2 \approx \mathrm{d}\rho^2 + \rho^2\mathrm{d}\phi^2 + a^2\mathrm{d}\theta^2, \tag{1a}$$

since, it is assumed that

$$|\bar{\rho}\cos\phi| \leqslant |\bar{\rho}| \ll 1; \quad \bar{\rho} = \frac{\rho}{a}. \tag{1b}$$

This assumption is consistent with the objective of investigation of the boundary layer effect caused by the presence of a penny shaped crack or anticrack in line with the Griffith–Irwin theory.

Since the local coordinate system (ρ, ϕ, θ) is orthogonal, the components of the Euclidean metric and associated metric tensors, g_{ij} and g^{ij}, $i, j = 1, 2, 3$, respectively, are given by

$$g_{11} = 1, \quad g_{22} = \rho^2, \quad g_{33} \approx a^2 \tag{2a}$$

and

$$g^{11} = 1, \quad g^{22} = \frac{1}{\rho^2}, \quad g^{33} \approx \frac{1}{a^2}; \tag{2b}$$

for $\rho \ll a$.

The nonvanishing components of the Christoffel three-index symbol of the second kind, associated with a scheme of measurement in a Riemann space, and defined by

$$\Gamma^i_{\alpha\beta} = \frac{1}{2} g^{i\sigma}\left(\frac{\partial g_{\alpha\beta}}{\partial x^\alpha} + \frac{\partial g_{\alpha\sigma}}{\partial x^\beta} - \frac{\partial g_{\alpha\beta}}{\partial x^\sigma}\right), \quad i, \alpha, \beta, \sigma = 1, 2, 3 \tag{3}$$

can be written as follows:

$$\Gamma^1_{22} = -\rho, \quad \Gamma^2_{12} = \Gamma^2_{21} = \frac{1}{\rho}. \tag{4}$$

The kinematic relations concerning the physical components of the engineering strain in terms of the physical components of the displacement vector can then be written as follows:

$$\begin{aligned} &\varepsilon_\rho = \frac{\partial U_\rho}{\partial \rho}, \quad \varepsilon_\phi = \frac{1}{\rho}\frac{\partial U_\phi}{\partial \phi} + \frac{U_\rho}{\rho}, \quad \varepsilon_\theta \approx \frac{1}{a}\frac{\partial U_\theta}{\partial \theta}, \quad \varepsilon_{\phi\theta} \approx \frac{1}{a}\frac{\partial U_\phi}{\partial \theta} + \frac{1}{\rho}\frac{\partial U_\theta}{\partial \phi}, \\ &\varepsilon_{\rho\theta} \approx \frac{\partial U_\theta}{\partial \rho} + \frac{1}{a}\frac{\partial U_\rho}{\partial \theta}, \quad \varepsilon_{\rho\phi} = \frac{1}{\rho}\frac{\partial U_\rho}{\partial \phi} + \frac{\partial U_\phi}{\partial \rho} - \frac{U_\phi}{\rho}; \quad \text{for } \rho \ll a. \end{aligned} \tag{5}$$

Substitution of the kinematic relations, given by Eq. (5) and linear elastic isotropic constitutive relations (Hooke's law) into the equilibrium equations,

$$\sigma_{\ell i/\ell} = 0; \quad i, \ell = 1, 2, 3, \tag{6}$$

in which the subscripts denote covariant components and / represents covariant differentiation, the equations of equilibrium (in the absence of body forces) in terms of the physical components of the displacement vector $U_{\rho j}$, $U_{\phi j}$, and $U_{\theta j}$, $j = 1, 2$, can be derived as given below ($\rho \ll a$):

$$\begin{aligned} &(\lambda + 2G)\frac{\partial^2 U_\rho}{\partial \rho^2} + \frac{(\lambda + 2G)}{\rho}\frac{\partial U_\rho}{\partial \rho} - (\lambda + 2G)\frac{U_\rho}{\rho^2} + \frac{G}{\rho^2}\frac{\partial^2 U_\rho}{\partial \phi^2} + \frac{(\lambda + G)}{\rho}\frac{\partial^2 U_\phi}{\partial \rho \partial \phi} - \frac{(\lambda + 3G)}{\rho^2}\frac{\partial U_\phi}{\partial \phi} \\ &\quad + \frac{G}{a^2}\frac{\partial^2 U_\rho}{\partial \theta^2} + \frac{(\lambda + G)}{a}\frac{\partial^2 U_\theta}{\partial \rho \partial \theta} = 0; \end{aligned} \tag{7a}$$

$$\begin{aligned} &\frac{(\lambda + G)}{\rho}\frac{\partial^2 U_\rho}{\partial \phi \partial \rho} + \frac{(\lambda + 3G)}{\rho^2}\frac{\partial U_\rho}{\partial \phi} + G\frac{\partial^2 U_\phi}{\partial \rho^2} + G\frac{\partial U_\phi}{\rho \partial \rho} - G\frac{U_\phi}{\rho^2} + (\lambda + 2G)\frac{\partial^2 U_\phi}{\rho^2 \partial \phi^2} + \frac{G}{a^2}\frac{\partial^2 U_\phi}{\partial \theta^2} \\ &\quad + \frac{(\lambda + G)}{a\rho}\frac{\partial^2 U_\theta}{\partial \phi \partial \theta} = 0; \end{aligned} \tag{7b}$$

$$\frac{(\lambda + G)}{a}\frac{\partial^2 U_\rho}{\partial \rho \partial \theta} + \frac{(\lambda + G)}{a}\frac{\partial U_\rho}{\rho \partial \theta} + \frac{(\lambda + G)}{a}\frac{\partial^2 U_\phi}{\rho \partial \phi \partial \theta} + \frac{(\lambda + 2G)}{a^2}\frac{\partial^2 U_\theta}{\partial \theta^2} + G\frac{\partial^2 U_\theta}{\partial \rho^2} + G\frac{\partial U_\theta}{\rho \partial \rho} + \frac{G}{\rho^2}\frac{\partial^2 U_\theta}{\partial \phi^2} = 0; \tag{7c}$$

where λ and G are Lame's constants. The correct solution must satisfy the governing partial differential equations and boundary conditions. The boundary conditions prescribed at the top and bottom surfaces of the penny shaped crack or thin rigid inclusion can be written as follows:

(i) Penny shaped crack:

$$\phi = \pm\pi: \quad \sigma_\phi = \tau_{\rho\phi} = \tau_{\phi\theta} = 0. \tag{8}$$

(ii) Penny shaped anticrack or perfectly bonded thin rigid inclusion:

$$\phi = \pm\pi: \quad U_\phi = U_\rho = U_\theta = 0. \tag{9}$$

(iii) Penny shaped thin transversely rigid inclusion (frictionless planar slip permitted):

$$\phi = \pm\pi: \quad U_\phi = \tau_{\rho\phi} = U_\theta = 0. \tag{10}$$

(iv) Penny shaped thin rigid inclusion in part perfectly bonded ($a \leqslant r \leqslant b$), the remainder with frictionless slip ($0 \leqslant r \leqslant a$) as shown in Fig. 2:
(a) For $r = a$:

$$\phi = 0: \quad U_\phi = U_\rho = U_\theta = 0; \tag{11a}$$

$$\phi = \pm\pi: \quad U_\phi = \tau_{\rho\phi} = \tau_{\phi\theta} = 0. \tag{11b}$$

(b) For $r = b$:
The boundary conditions and analytical procedure are the same those for the anticrack (Case (ii)) discussed above, except that a is replaced by b in the derivation, and hence will not be discussed further.

(v) Penny shaped thin rigid inclusion alongside penny shaped crack:

$$\phi = \pi: \quad U_\phi = U_\rho = U_\theta = 0; \tag{12a}$$

$$\phi = -\pi: \quad \sigma_\phi = \tau_{\rho\phi} = \tau_{\phi\theta} = 0. \tag{12b}$$

The solution sought must satisfy the governing equations (7) and one of the five combinations of boundary conditions (8)–(12) listed above.

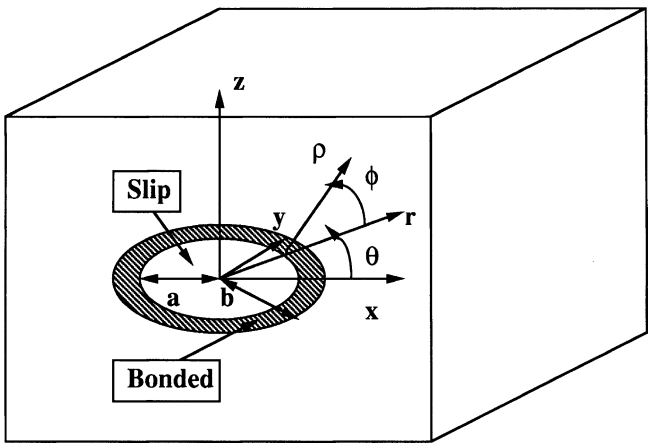

Fig. 2. Penny shaped thin rigid inclusion in part perfectly bonded, the remainder with slip.

3. Solution strategy

The assumed displacement functions for the three-dimensional plate problem under consideration are selected on the basis of separation of variables in a manner similar to their counterparts for the three-dimensional crack problem investigated earlier by Chaudhuri and Xie (2000). These are as given below:

$$U_\rho(\rho,\phi,\theta) = \mathrm{e}^{\mathrm{i}\alpha\theta}\Phi_\rho(\phi)R_\rho(\rho) = \mathrm{e}^{\mathrm{i}\alpha\theta+p\phi}R_\rho(\rho); \tag{13a}$$

$$U_\phi(\rho,\phi,\theta) = \mathrm{e}^{\mathrm{i}\alpha\theta}\Phi_\phi(\phi)R_\phi(\rho) = \mathrm{e}^{\mathrm{i}\alpha\theta+p\phi}R_\phi(\rho); \tag{13b}$$

$$U_\theta(\rho,\phi,\theta) = \mathrm{e}^{\mathrm{i}\alpha\theta}\Phi_\theta(\phi)R_\theta(\rho) = \mathrm{e}^{\mathrm{i}\alpha\theta+p\phi}R_\theta(\rho); \tag{13c}$$

where $\alpha \in Z$, the set of integers. It may be noted that since the θ-dependent term is nonsingular and periodic, it can be best represented by Fourier series. Substitution of Eq. (13) into Eq. (7) yields the following system of coupled ordinary differential equations (ODE's) valid for $\rho \ll a$:

$$(\lambda+2G)\frac{\mathrm{d}^2R_\rho}{\mathrm{d}\rho_1^2} + \frac{(\lambda+2G)}{\rho_1}\frac{\mathrm{d}R_\rho}{\mathrm{d}\rho_1} - (\lambda+2G)\frac{R_\rho}{\rho_1^2} + \frac{G}{\rho_1^2}p^2R_\rho + \frac{(\lambda+G)}{\rho_1}p\frac{\mathrm{d}R_\phi}{\mathrm{d}\rho_1} - \frac{(\lambda+3G)}{\rho_1^2}pR_\phi + GR_\rho + (\lambda+G)\frac{\mathrm{d}R_\theta}{\mathrm{d}\rho_1} = 0; \tag{14a}$$

$$\frac{(\lambda+G)}{\rho_1}p\frac{\mathrm{d}R_\rho}{\mathrm{d}\rho_1} + \frac{(\lambda+3G)}{\rho_1^2}pR_\rho + G\frac{\mathrm{d}^2R_\phi}{\mathrm{d}\rho_1^2} + \frac{G}{\rho_1}\frac{\mathrm{d}R_\phi}{\mathrm{d}\rho_1} - \frac{G}{\rho_1^2}R_\phi + \frac{(\lambda+2G)}{\rho_1^2}p^2R_\phi + GR_\phi + \frac{(\lambda+G)}{\rho_1}pR_\theta = 0; \tag{14b}$$

$$(\lambda+G)\frac{\mathrm{d}R_\rho}{\mathrm{d}\rho_1} + \frac{(\lambda+G)}{\rho_1}R_\rho + \frac{(\lambda+G)}{\rho_1}pR_\phi + (\lambda+2G)R_\theta + G\frac{\mathrm{d}^2R_\theta}{\mathrm{d}\rho_1^2} + \frac{G}{\rho_1}\frac{\mathrm{d}R_\theta}{\mathrm{d}\rho_1} + \frac{G}{\rho_1^2}p^2R_\theta = 0; \tag{14c}$$

where

$$\rho_1 = \mathrm{i}\alpha(\rho/a). \tag{15}$$

4. Asymptotic stress field corresponding to far-field torsional shear (mode III) loading

This case has not been investigated by earlier researchers, e.g., Sneddon (1946). Although Fig. 1 shows the far-field loadings in Cartesian coordinates, the geometry of the penny shaped discontinuity necessitates employment of the cylindrical polar coordinate system, to describe far-field loads responsible for the growth of a penny shaped crack under modes I, II and III loading conditions, schematically shown in Fig. 3. The far-field loading, that corresponds to torsional or antiplane (with respect to the ρ–ϕ plane) shear (mode III) load, is the torsional shear stress $\tau_{\theta z}^{\infty}$, which is applied on the top face of a cylinder of radius d, $d \to \infty$, weakened/reinforced by a penny shaped discontinuity of radius, a, while the bottom face of the cylinder is clamped (Fig. 3). Transformation to the local coordinates ρ, ϕ, θ, followed by the use of Hooke's law and kinematic relations, given by Eq. (5), will clearly demonstrate that the most dominant stress singularity under mode III far-field loading will arise out of the displacement component, U_θ. The solution to the system of coupled ODE's (14) can now be assumed in the form of the Frobenius type series solutions (Chaudhuri and Xie, 2000), such that the displacement component, U_θ, has the lowest exponent of ρ, for s and n positive, thus yielding the dominant torsional shear stress singularity ($\rho \ll a$):

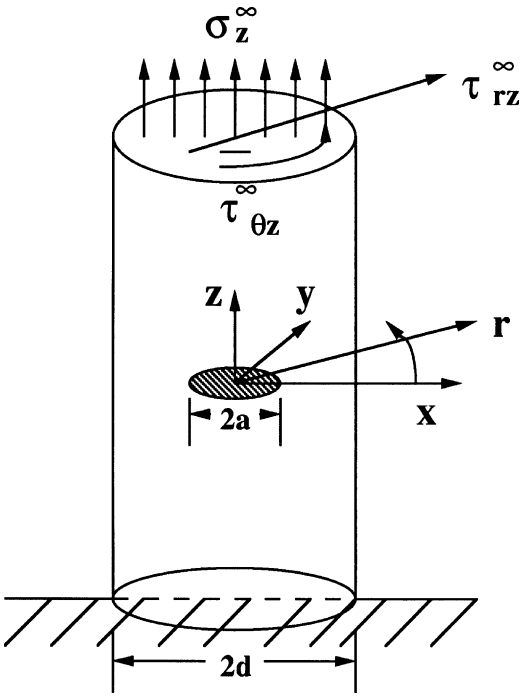

Fig. 3. Far-field loadings σ_z^∞ (mode I), τ_{rz}^∞ (mode II) and $\tau_{\theta z}^\infty$ (mode III) in cylindrical polar coordinates.

$$R_\rho = \sum_{n=0}^{\infty} a_{s+2n}\rho_1^{s+2n+1}; \quad R_\phi = \sum_{n=0}^{\infty} b_{s+2n}\rho_1^{s+2n+1}; \quad R_\theta = \sum_{n=0}^{\infty} c_{s+2n}\rho_1^{s+2n}. \tag{16}$$

Substitution of Eq. (16) into Eq. (14) yields a recurrent relationship, which, for $n = 0$, supplies the following characteristic equation for the coupled differential equations:

$$s^2 + p^2 = 0 \quad \text{leading to } p_{1,2} = \pm \mathrm{i}s. \tag{17}$$

This permits the ϕ-dependent term to be written in the form:

$$\Phi_\theta(\phi) = (\overline{\overline{A}}_1 \sin(s\phi) + \overline{\overline{A}}_2 \cos(s\phi)), \tag{18a}$$

$$\Phi_\rho(\phi) = (\overline{\overline{A}}_1 \sin(s\phi) + \overline{\overline{A}}_2 \cos(s\phi)), \tag{18b}$$

$$\Phi_\phi(\phi) = (\overline{\overline{A}}_1 \cos(s\phi) - \overline{\overline{A}}_2 \sin(s\phi)). \tag{18c}$$

In addition, since a θ-dependent term is, as mentioned earlier, assumed in the form of a Fourier series, the assumed displacement functions can be written as follows:

$$U_\theta = I_{1s}\left(\overline{D}_1 \cos(\alpha\theta) + \overline{D}_2 \mathrm{i} \sin(\alpha\theta)\right)\left(\overline{\overline{A}}_1 \sin(s\phi) + \overline{\overline{A}}_2 \cos(s\phi)\right), \tag{19a}$$

$$U_\rho = -I_{2s+1}\left(\overline{D}_1 \mathrm{i} \sin(\alpha\theta) + \overline{D}_2 \cos(\alpha\theta)\right)\left(\overline{\overline{A}}_1 \sin(s\phi) + \overline{\overline{A}}_2 \cos(s\phi)\right), \tag{19b}$$

$$U_\phi = I_{3s+1}\left(\overline{D}_1 \mathrm{i} \sin(\alpha\theta) + \overline{D}_2 \cos(\alpha\theta)\right)\left(\overline{\overline{A}}_1 \cos(s\phi) - \overline{\overline{A}}_2 \sin(s\phi)\right), \tag{19c}$$

where

$$I_{1s} = \sum_{n=0}^{\infty} c_{s+2n}\rho_1^{s+2n}; \quad I_{2s+1} = \sum_{n=0}^{\infty} a_{s+2n}\rho_1^{s+2n+1}; \quad I_{3s+1} = \sum_{n=0}^{\infty} b_{s+2n}\rho_1^{s+2n+1}. \tag{20}$$

The general recurrent relationship for the coefficients, a_s, b_s, c_s, is given by

$$a_{s+2n}[-(\lambda+2G)(s+2n+2)(s+2n)+Gs^2] + b_{s+2n}s[-(\lambda+G)(s+2n+1)+(\lambda+3G)] - a_{s+2n-2}G + c_{s+2n}(\lambda+G)(s+2n) = 0, \tag{21a}$$

$$-a_{s+2n}s[(\lambda+G)(s+2n+1)+(\lambda+3G)] + b_{s+2n}[G(s+2n+2)(s+2n)-(\lambda+2G)s^2] + Gb_{s+2n-2} + c_{s+2n}s(\lambda+G) = 0, \tag{21b}$$

$$-a_{s+2n-2}(\lambda+G)(s+2n) - b_{s+2n-2}(\lambda+G)s + c_{s+2n-2}(\lambda+2G) + c_{s+2n}G((s+2n)^2 - s^2) = 0. \tag{21c}$$

When $n = 0$, both Eqs. (21a) and (21b) reduce to

$$a_s[(\lambda+G)s+2(\lambda+2G)] + b_s[(\lambda+G)(s+1)-\lambda-3G] = (\lambda+G)c_s. \tag{22}$$

The general asymptotic form for the transverse displacement component, U_θ, can be written as follows ($\rho \ll a$):

$$U_\theta = \frac{\rho^s B_b(\theta)}{G}(A_1\sin(s\phi) + A_2\cos(s\phi)) + \mathrm{O}(\bar{\rho}^{s+2}); \tag{23a}$$

$$U_\rho = \mathrm{O}(\bar{\rho}^{s+1}), \quad U_\phi = \mathrm{O}(\bar{\rho}^{s+1}); \tag{23b}$$

where

$$B_b(\theta) = \sum_{\alpha=0,1,2,\ldots,}^{\infty} (D_{1\alpha}\cos(\alpha\theta) + D_{2\alpha}\sin(\alpha\theta)), \tag{24}$$

and

$$A_{1,2} = Gc_s\overline{\overline{A}}_{1,2}; \quad D_1 = (\mathrm{i}\alpha)^s\overline{D}_1, \quad D_2 = \mathrm{i}(\mathrm{i}\alpha)^s\overline{D}_2; \tag{25}$$

wherein α is arbitrary. The asymptotic stress field can be obtained from Eq. (23) as follows ($\rho \ll a$):

$$\tau_{\phi\theta} = \rho^{s-1}B_b(\theta)s(A_1\cos(s\phi) - A_2\sin(s\phi)) + \mathrm{O}(\bar{\rho}^{s+1}), \tag{26a}$$

$$\tau_{\rho\theta} = \rho^{s-1}B_b(\theta)s(A_1\sin(s\phi) + A_2\cos(s\phi)) + \mathrm{O}(\bar{\rho}^{s+1}), \tag{26b}$$

$$\tau_{\rho\phi} = \mathrm{O}(\bar{\rho}^s), \quad \sigma_\rho = \mathrm{O}(\bar{\rho}^s), \quad \sigma_\phi = \mathrm{O}(\bar{\rho}^s), \quad \sigma_\theta = \mathrm{O}(\bar{\rho}^s). \tag{26c}$$

It may be noted that since s is positive, all the higher order terms in Eq. (26) vanish as $\rho \to 0$. This is consistent with the asymptotic expansion for the two-dimensional crack problem due to Williams (1957).

The asymptotic stress field, given above by Eqs. (23) and (26) can easily be transformed into the corresponding cylindrical polar coordinate system (r, θ, z) by using the transformation relations:

$$\begin{Bmatrix} \tau_{r\theta} \\ \tau_{\theta z} \end{Bmatrix} = \begin{bmatrix} \cos\phi & \sin\phi \\ -\sin\phi & \cos\phi \end{bmatrix} \begin{Bmatrix} \tau_{\rho\theta} \\ \tau_{\phi\theta} \end{Bmatrix}; \tag{27a}$$

$$\sigma_z = \mathrm{O}(\bar{\rho}^s), \quad \sigma_r = \mathrm{O}(\bar{\rho}^s), \quad \tau_{rz} = \mathrm{O}(\bar{\rho}^s), \quad \sigma_\theta = \mathrm{O}(\bar{\rho}^s). \tag{27b}$$

4.1. Penny shaped discontinuity-surface boundary conditions

The expressions for stresses and displacements also need to satisfy the boundary conditions prescribed on the top and bottom surfaces of the penny shaped crack or anticrack. The five combinations, as given by Eqs. (8)–(12), are considered below:

(i) Penny shaped crack:

Substitution of Eq. (26a) into Eq. (8) supplies the following characteristic equation:

$$\sin(2s\pi) = 0. \tag{28}$$

The above yields the minimum root (eigenvalue), contributing to the singular stresses, $s = 1/2$.

It must be stressed that strength of the stress singularity remains unchanged throughout the plate thickness. The stress distribution in the vicinity of a penny-shaped crack front, i.e., $\rho \ll a$, can be expressed as follows:

$$\tau_{\rho\theta}(\rho, \phi, \theta) = \frac{K_{\mathrm{III}}}{\sqrt{2\pi\rho}} \sin(\phi/2); \tag{29a}$$

$$\tau_{\phi\theta}(\rho, \phi, \theta) = \frac{K_{\mathrm{III}}}{\sqrt{2\pi\rho}} \cos(\phi/2); \tag{29b}$$

while the tangential displacement component is given by

$$U_{\theta}(\rho, \phi, \theta) = \frac{2K_{\mathrm{III}}(\theta)}{G} \sqrt{\frac{\rho}{2\pi}} \sin\left(\frac{\phi}{2}\right), \tag{30}$$

where

$$K_{\mathrm{III}}(\theta) = K_{\mathrm{IIIs}}(\theta) + K_{\mathrm{IIIa}}(\theta); \tag{31}$$

with

$$K_{\mathrm{IIIs}}(\theta) = \sqrt{\frac{\pi}{2}} A_1 B_{b\mathrm{s}}(\theta); \tag{32a}$$

$$K_{\mathrm{IIIa}}(\theta) = \sqrt{\frac{\pi}{2}} A_1 B_{b\mathrm{a}}(\theta). \tag{32b}$$

Thus, the stress intensity factor for mode III can be separated into symmetric (K_{IIIs}) and anti-symmetric (K_{IIIa}) parts.

(ii) Penny shaped anticrack or perfectly bonded thin rigid inclusion:

Substitution of Eq. (23a) into Eq. (9) supplies the following characteristic equation:

$$\sin(2s\pi) = 0. \tag{33}$$

The above yields the minimum root (eigenvalue), contributing to the singular stresses, $s = 1/2$.

The stress distribution in the vicinity of a semi-infinite anticrack front, i.e., $\rho \ll a$, can be expressed as follows:

$$\tau_{\rho\theta}(\rho, \phi, \theta) = \frac{K_{\mathrm{III}}^{(i)}(\theta)}{\sqrt{2\pi\rho}} \cos(\phi/2), \tag{34a}$$

$$\tau_{\phi\theta}(\rho, \phi, \theta) = -\frac{K_{\mathrm{III}}^{(i)}(\theta)}{\sqrt{2\pi\rho}} \sin(\phi/2); \tag{34b}$$

while the tangential displacement component is given by

$$U_\theta(\rho,\phi,\theta) = \frac{2K_{\mathrm{III}}^{(i)}(\theta)}{G}\sqrt{\frac{\rho}{2\pi}}\cos\left(\frac{\phi}{2}\right), \tag{35}$$

where

$$K_{\mathrm{III}}^{(i)}(\theta) = K_{\mathrm{IIIs}}^{(i)}(\theta) + K_{\mathrm{IIIa}}^{(i)}(\theta), \tag{36}$$

with

$$K_{\mathrm{IIIs}}^{(i)}(\theta) = \sqrt{\frac{\pi}{2}}A_2 B_{bs}(\theta), \tag{37a}$$

$$K_{\mathrm{IIIa}}^{(i)}(\theta) = \sqrt{\frac{\pi}{2}}A_2 B_{ba}(\theta). \tag{37b}$$

Thus, the stress intensity factor for mode III can be separated into symmetric ($K_{\mathrm{IIIs}}^{(i)}$) and anti-symmetric ($K_{\mathrm{IIIa}}^{(i)}$) parts.

(iii) Penny shaped thin transversely rigid inclusion (frictionless planar slip permitted):

Substitution of Eq. (23a) into Eq. (10) supplies the same characteristic equation as in the case of an anticrack (see (ii) above). The mode III stress intensity factors are also identical, and will not be repeated here.

(iv) Penny shaped thin rigid inclusion in part perfectly bonded, the remainder with frictionless slip (Fig. 2):

Substitution of Eq. (26a) into Eq. (11b) supplies the same characteristic equation as in the case of a penny shaped crack discussed in (i) above. It may be noted here that the interface continuity condition, given by Eq. (11a) is automatically satisfied. The mode III stress intensity factors are also identical to their counterparts for a penny shaped crack, and will not be repeated here.

(v) Penny shaped thin rigid inclusion alongside penny shaped crack:

Substitution of Eqs. (23a) and (26a) into Eqs. (12a) and (12b), respectively, yields the following characteristic equation:

$$\cos(2s\pi) = 0. \tag{38}$$

The minimum roots (eigenvalue) contributing to the singular stresses are:

$$s_1 = \frac{1}{4}; \quad s_2 = \frac{3}{4}. \tag{39}$$

The singular parts of $\tau_{\rho\theta}$ and $\tau_{\phi\theta}$ are given by

$$\tau_{\rho\theta}, \tau_{\phi\theta} \sim \mathrm{O}(\rho^{-3/4}) + \mathrm{O}(\rho^{-1/4}). \tag{40}$$

5. Asymptotic stress fields corresponding to far-field extension–bending (mode I)/sliding shear–twisting (mode II) loadings

The case of sliding shear/twisting (mode II) has not been investigated by earlier researchers, e.g., Sneddon (1946), who have discussed the case of extension/bending (mode I) only. As before, although Fig. 1 shows the far-field loadings in Cartesian coordinates, the geometry of the penny shaped discontinuity necessitates employment of the cylindrical polar coordinate system, to describe far-field loads responsible

for the growth of a penny shaped crack under modes I, II and III loading conditions, schematically shown in Fig. 3. The far-field loadings, that correspond to extension/bending (mode I) and inplane (with respect to the $\rho-\phi$ plane) sliding shear/twisting (mode II) loads, are given by the normal stress, σ_z^{∞}, and shear stress, τ_{rz}^{∞}, respectively, applied on the top face of a cylinder of radius d, $d\to\infty$, weakened/reinforced by a penny shaped discontinuity of radius, a, while the bottom face of the cylinder is clamped (Fig. 3). Transformation to the local coordinates ρ, ϕ, θ, followed by the use of Hooke's law and kinematic relations, given by Eq. (5), will clearly demonstrate that the most dominant stress singularity under mode I and II far-field loading will arise out of the displacement components, U_ρ and U_ϕ. The solution to the system of coupled ODE's (14) can now be assumed in the form of the Frobenius type series solutions (Chaudhuri and Xie, 2000), such that the displacement components, U_ρ and U_ϕ, have the lowest exponent of ρ, for s and n positive, thus yielding the dominant opening normal stress, σ_z, and sliding shear stress, τ_{rz}, singularities ($\rho\ll a$):

$$R_\rho(\rho_1)=\sum_{n=0}^{\infty}a_{s+n}\rho_1^{s+2n};\quad R_\phi(\rho_1)=\sum_{n=0}^{\infty}b_{s+n}\rho_1^{s+2n};\quad R_\theta(\rho_1)=\sum_{n=0}^{\infty}c_{s+n}\rho_1^{s+2n+1}. \tag{41}$$

On substitution of Eq. (41) into Eq. (14), a set of recurrent relationships can be derived. When $n=0$, the characteristic equations for the coupled differential equations are given by

$$a_s[(\lambda+2G)(s^2-1)+Gp^2]+b_sp[(\lambda+G)s-(\lambda+3G)]=0, \tag{42a}$$

$$a_sp[s(\lambda+G)+(\lambda+3G)]+b_s[G(s^2-1)+(\lambda+2G)p^2]=0. \tag{42b}$$

The above equations are found to have four imaginary roots:

$$p_{1,2}=\pm\mathrm{i}(s+1),\quad p_{3,4}=\pm\mathrm{i}(s-1). \tag{43}$$

The final results that satisfy the equilibrium equations (7) can be expressed in the following form:

$$U_\rho=U_{\rho1}+U_{\rho2};\quad U_\phi=U_{\phi1}+U_{\phi2};\quad U_\theta=U_{\theta1}+U_{\theta2}; \tag{44}$$

where

$$U_{\rho1}=I_s(\overline{\overline{D}}_{1\alpha}\mathrm{i}\sin(\alpha\theta)+\overline{\overline{D}}_{2\alpha}\cos(\alpha\theta))(\overline{A}_1\sin(s+1)\phi+\overline{A}_2\cos(s+1)\phi); \tag{45a}$$

$$U_{\phi1}=I_s(\overline{\overline{D}}_{1\alpha}\mathrm{i}\sin(\alpha\theta)+\overline{\overline{D}}_{2\alpha}\cos(\alpha\theta))(\overline{A}_1\cos(s+1)\phi-\overline{A}_2\sin(s+1)\phi); \tag{45b}$$

$$U_{\theta1}=I_{s+1}(\overline{\overline{D}}_{1\alpha}\cos(\alpha\theta)+\overline{\overline{D}}_{2\alpha}\mathrm{i}\sin(\alpha\theta))(\overline{A}_1\sin(s+1)\phi+\overline{A}_2\cos(s+1)\phi) \tag{45c}$$

and

$$U_{\rho2}=I_{s1}(\overline{\overline{D}}_{1\alpha}\mathrm{i}\sin(\alpha\theta)+\overline{\overline{D}}_{2\alpha}\cos(\alpha\theta))(\overline{A}_3\sin(s-1)\phi+\overline{A}_4\cos(s-1)\phi); \tag{46a}$$

$$U_{\phi2}=I_{s1}(\overline{\overline{D}}_{1\alpha}\mathrm{i}\sin(\alpha\theta)+\overline{\overline{D}}_{2\alpha}\cos(\alpha\theta))(\overline{A}_3\cos(s-1)\phi-\overline{A}_4\sin(s-1)\phi); \tag{46b}$$

$$U_{\theta2}=I_{s3}(\overline{\overline{D}}_{1\alpha}\cos(\alpha\theta)+\overline{\overline{D}}_{2\alpha}\mathrm{i}\sin(\alpha\theta))(\overline{A}_3\sin(s-1)\phi+\overline{A}_4\cos(s-1)\phi); \tag{46c}$$

in which I_s and I_{s+1} are modified Bessel's functions of the first kind, while I_{s1}, I_{s2}, I_{s3} are in the form as given below:

$$I_{s1}=\sum_{n=0}^{\infty}a_{s+2n}\rho_1^{s+2n};\quad I_{s2}=\sum_{n=0}^{\infty}b_{s+2n}\rho_1^{s+2n};\quad I_{s3}=\sum_{n=0}^{\infty}c_{s+2n}\rho_1^{s+2n+1}. \tag{47}$$

The general recurrent relationship for the coefficients, a_{s+2n}, b_{s+2n}, c_{s+2n}, is given by

$$a_{s+2n}[(\lambda+2G)(s+2n+1)(s+2n-1)-G(s-1)^2]-b_{s+2n}(s-1)[(\lambda+G)(s+2n)-(\lambda+3G)] + a_{s+2n-2}G+c_{s+2n-2}(\lambda+G)(s+2n-1)=0, \tag{48a}$$

$$a_{s+2n}(s-1)[(\lambda+G)(s+2n)+(\lambda+3G)]+b_{s+2n}[G(s+2n+1)(s+2n-1)-(\lambda+2G)(s-1)^2] + b_{s+2n-2}G+c_{s+2n-2}(\lambda+G)(s-1)=0, \tag{48b}$$

$$a_{s+2n}(\lambda+G)(s+2n+1)-b_{s+2n}(\lambda+G)(s-1)+c_{s+2n-2}(\lambda+2G)+c_{s+2n}G[(s+2n+1)^2-(s-1)^2]=0. \tag{48c}$$

The asymptotic forms of Eqs. (44)–(46) are given as follows ($\rho \ll a$):

$$U_\rho=\rho_1^s\left[\frac{2^{-s}}{\Gamma(s+1)}(A_1'(\theta)\sin(s+1)\phi+A_2'(\theta)\cos(s+1)\phi)+a_s(A_{3j}'(\theta)\sin(s-1)\phi + A_4'(\theta)\cos(s-1)\phi)\right]+\mathrm{O}(\bar{\rho}^{s+2}); \tag{49a}$$

$$U_\phi=\rho_1^s\left[\frac{2^{-s}}{\Gamma(s+1)}(A_1'(\theta)\cos(s+1)\phi-A_2'(\theta)\sin(s+1)\phi)+f_1a_s(A_3'(\theta)\cos(s-1)\phi - A_4'(\theta)\sin(s-1)\phi)\right]+\mathrm{O}(\bar{\rho}^{s+2}); \tag{49b}$$

$$U_\theta=\mathrm{O}(\bar{\rho}^{s+1}); \tag{49c}$$

where

$$f_1=\frac{(\lambda+G)s+(\lambda+3G)}{(\lambda+G)s-(\lambda+3G)} \tag{50}$$

and

$$A_i'(\theta)=\overline{A}_iB_1(\theta),\quad i=1,2,3,4; \tag{51}$$

in which

$$B_1(\theta)=\sum_{\alpha=0,1,2}^{\infty}(D_{1\alpha}\sin(\alpha\theta)+D_{2\alpha}\cos(\alpha\theta)), \tag{52a}$$

with

$$D_{1\alpha}=\mathrm{i}\overline{\overline{D}}_{1\alpha},\quad D_{2\alpha}=\overline{\overline{D}}_{2\alpha}. \tag{52b}$$

The displacement and stress fields in the vicinity of the tip of a penny shaped crack or anticrack can be written down in the form ($\rho \ll a$):

$$U_\rho=\frac{\rho^s}{2Gs}[(A_1(\theta)\sin(s+1)\phi+A_2(\theta)\cos(s+1)\phi)+(s-3+4v)(A_3(\theta)\sin(s-1)\phi + A_4(\theta)\cos(s-1)\phi)]+\mathrm{O}(\bar{\rho}^{s+2}); \tag{53a}$$

$$U_\phi=\frac{\rho^s}{2Gs}[(A_1(\theta)\cos(s+1)\phi-A_2(\theta)\sin(s+1)\phi)+(s+3-4v)(A_3(\theta)\cos(s-1)\phi - A_4(\theta)\sin(s-1)\phi)]+\mathrm{O}(\bar{\rho}^{s+2}); \tag{53b}$$

$$U_\theta = \mathrm{O}(\bar{\rho}^{s+1}) \tag{53c}$$

and

$$\sigma_\rho = \rho^{s-1}[(A_1(\theta)\sin(s+1)\phi + A_2(\theta)\cos(s+1)\phi) + (s-3)(A_3(\theta)\sin(s-1)\phi + A_4(\theta)\cos(s-1)\phi)] + \mathrm{O}(\bar{\rho}^{s+1}); \tag{54a}$$

$$\sigma_\phi = -\rho^{s-1}[(A_1(\theta)\sin(s+1)\phi + A_2(\theta)\cos(s+1)\phi) + (s+1)(A_3(\theta)\sin(s-1)\phi + A_4(\theta)\cos(s-1)\phi)] + \mathrm{O}(\bar{\rho}^{s+1}); \tag{54b}$$

$$\tau_{\rho\phi} = \rho^{s-1}[(A_1(\theta)\cos(s+1)\phi - A_2(\theta)\sin(s+1)\phi) + (s-1)(A_3(\theta)\cos(s-1)\phi - A_4(\theta)\sin(s-1)\phi)] + \mathrm{O}(\bar{\rho}^{s+1}); \tag{54c}$$

$$\sigma_\theta = -4\nu\rho^{s-1}(A_3(\theta)\sin(s-1)\phi + A_4(\theta)\cos(s-1)\phi) + \mathrm{O}(\bar{\rho}^{s+1}); \tag{54d}$$

$$\tau_{\rho\theta} = \mathrm{O}(\bar{\rho}^{s}), \quad \tau_{\phi\theta} = \mathrm{O}(\bar{\rho}^{s}); \tag{54e}$$

where

$$A_{1,2}(\theta) = \left(\mathrm{i}\frac{\alpha}{a}\right)^s \frac{Gs}{2^{s-1}\Gamma(s+1)} A'_{1,2}(\theta); \tag{55a}$$

$$A_{3,4}(\theta) = \left(\mathrm{i}\frac{\alpha}{a}\right)^s \frac{2sG(\lambda+G)a_s}{(\lambda+G)s - (\lambda+3G)} A'_{3,4}(\theta). \tag{55b}$$

It may be noted that since s or $\mathrm{Re}\, s$ (when s is complex) is positive, all the higher order terms in Eq. (54), vanish as $\rho \to 0$. This is consistent with the asymptotic expansion for the two-dimensional crack problem due to Williams (1957). It may further be noted that the present governing partial differential equations (7) and the resulting solutions are approximated to be valid only in the immediate vicinity of the penny shaped discontinuity ($\bar{\rho} \ll 1$).

The asymptotic displacement and stress fields, given above by Eqs. (53) and (54) can easily be transformed into the corresponding cylindrical polar coordinate system (r, θ, z) by using the following transformation (refer to Fig. 1):

$$\rho\sin\phi = z; \quad \rho\cos\phi = r - a; \tag{56}$$

$$\begin{Bmatrix} U_r \\ U_z \end{Bmatrix} = \begin{bmatrix} \cos\phi & \sin\phi \\ -\sin\phi & \cos\phi \end{bmatrix} \begin{Bmatrix} U_\rho \\ U_\phi \end{Bmatrix}; \tag{57}$$

$$\begin{Bmatrix} \sigma_r \\ \sigma_z \\ \tau_{rz} \end{Bmatrix} = \begin{bmatrix} \cos^2\phi & \sin^2\phi & -\sin 2\phi \\ \sin^2\phi & \cos^2\phi & \sin 2\phi \\ \frac{1}{2}\sin 2\phi & -\frac{1}{2}\sin 2\phi & \cos 2\phi \end{bmatrix} \begin{Bmatrix} \sigma_\rho \\ \sigma_\phi \\ \tau_{\rho\phi} \end{Bmatrix}. \tag{58}$$

The remaining displacement and stress components are

$$\sigma_\theta = -4\nu\rho^{s-1}(A_3(\theta)\sin(s-1)\phi + A_4(\theta)\cos(s-1)\phi) + \mathrm{O}(\bar{\rho}^{s+1});$$

$$U_\theta = \mathrm{O}(\bar{\rho}^{s+1}); \quad \tau_{r\theta} = \mathrm{O}(\bar{\rho}^{s}); \quad \tau_{\theta z} = \mathrm{O}(\bar{\rho}^{s}). \tag{59}$$

These asymptotic displacement and stress fields can further be transformed into the corresponding Cartesian coordinate system (x, y, z) as follows:

$$\begin{Bmatrix} U_x \\ U_y \end{Bmatrix} = \begin{bmatrix} \cos\theta & -\sin\theta \\ \sin\theta & \cos\theta \end{bmatrix} \begin{Bmatrix} U_r \\ U_\theta \end{Bmatrix}; \tag{60}$$

$$\begin{Bmatrix} \sigma_x \\ \sigma_y \\ \tau_{xy} \end{Bmatrix} = \begin{bmatrix} \cos^2\theta & \sin^2\theta & -\sin 2\theta \\ \sin^2\theta & \cos^2\theta & \sin 2\theta \\ \frac{1}{2}\sin 2\theta & -\frac{1}{2}\sin 2\theta & \cos 2\theta \end{bmatrix} \begin{Bmatrix} \sigma_r \\ \sigma_\theta \\ \tau_{r\theta} \end{Bmatrix}; \tag{61a}$$

$$\begin{Bmatrix} \tau_{xz} \\ \tau_{yz} \end{Bmatrix} = \begin{bmatrix} \cos\theta & -\sin\theta \\ \sin\theta & \cos\theta \end{bmatrix} \begin{Bmatrix} \tau_{rz} \\ \tau_{\theta z} \end{Bmatrix}. \tag{61b}$$

The displacement component, U_z, and stress component, σ_z, are as given in Eqs. (57) and (58), respectively.

5.1. Penny shaped discontinuity-surface boundary conditions

The expressions for stresses and displacements derived above also need to satisfy the boundary conditions on the penny shaped crack or anticrack surfaces. The eigenvalues, which are related to the strength of the stress singularity (if any), can be obtained from these relations. On substitution of Eqs. (53) and (54) into the boundary conditions on the penny shaped crack or anticrack surfaces given by Eqs. (8)–(12) the eigenvalues for different boundary conditions can be obtained as follows:

(i) Penny shaped crack:

On substitution of Eqs. (54b,c) into the boundary conditions on the top and bottom surfaces of a penny shaped crack, given by Eq. (8), the computed minimum eigenvalue is given as $s = 1/2$. The stress distribution in the vicinity of the circular tip of a penny shaped crack, i.e., $\rho \ll a$, can, therefore, be expressed as follows:

$$\sigma_\rho(\rho,\phi,\theta) = \frac{K_{\mathrm{I}}(\theta)}{\sqrt{2\pi\rho}}\left(-\frac{1}{4}\cos\left(\frac{3\phi}{2}\right)+\frac{5}{4}\cos\left(\frac{\phi}{2}\right)\right)+\frac{K_{\mathrm{II}}(\theta)}{\sqrt{2\pi\rho}}\left(\frac{3}{4}\sin\left(\frac{3\phi}{2}\right)-\frac{5}{4}\sin\left(\frac{\phi}{2}\right)\right), \tag{62a}$$

$$\sigma_\phi(\rho,\phi,\theta) = \frac{K_{\mathrm{I}}(\theta)}{\sqrt{2\pi\rho}}\left(\frac{1}{4}\cos\left(\frac{3\phi}{2}\right)+\frac{3}{4}\cos\left(\frac{\phi}{2}\right)\right)-\frac{K_{\mathrm{II}}(\theta)}{\sqrt{2\pi\rho}}\left(\frac{3}{4}\sin\left(\frac{3\phi}{2}\right)+\frac{3}{4}\sin\left(\frac{\phi}{2}\right)\right), \tag{62b}$$

$$\tau_{\rho\phi}(\rho,\phi,\theta) = \frac{K_{\mathrm{I}}(\theta)}{\sqrt{2\pi\rho}}\left(\frac{1}{4}\sin\left(\frac{3\phi}{2}\right)+\frac{1}{4}\sin\left(\frac{\phi}{2}\right)\right)+\frac{K_{\mathrm{II}}(\theta)}{\sqrt{2\pi\rho}}\left(\frac{3}{4}\cos\left(\frac{3\phi}{2}\right)+\frac{1}{4}\cos\left(\frac{\phi}{2}\right)\right), \tag{62c}$$

$$\sigma_\theta(\rho,\phi,\theta) = \frac{2\nu K_{\mathrm{I}}(\theta)}{\sqrt{2\pi\rho}}\cos\left(\frac{\phi}{2}\right)-\frac{2\nu K_{\mathrm{II}}(\theta)}{\sqrt{2\pi\rho}}\sin\left(\frac{\phi}{2}\right) \tag{62d}$$

and

$$\begin{aligned} U_\rho(\rho,\phi,\theta) = &-\frac{K_{\mathrm{I}}(\theta)}{G}\sqrt{\frac{\rho}{2\pi}}\left(\frac{1}{4}\cos\left(\frac{3\phi}{2}\right)+\frac{-5+8\nu}{4}\cos\left(\frac{\phi}{2}\right)\right) \\ &+\frac{K_{\mathrm{II}}(\theta)}{G}\sqrt{\frac{\rho}{2\pi}}\left(\frac{3}{4}\sin\left(\frac{3\phi}{2}\right)+\frac{-5+8\nu}{4}\sin\left(\frac{\phi}{2}\right)\right), \end{aligned} \tag{63a}$$

$$\begin{aligned} U_\phi(\rho,\phi,\theta) = &\frac{K_{\mathrm{I}}(\theta)}{G}\sqrt{\frac{\rho}{2\pi}}\left(\frac{1}{4}\sin\left(\frac{3\phi}{2}\right)+\frac{-7+8\nu}{4}\sin\left(\frac{\phi}{2}\right)\right) \\ &+\frac{K_{\mathrm{II}}(\theta)}{G}\sqrt{\frac{\rho}{2\pi}}\left(\frac{3}{4}\cos\left(\frac{3\phi}{2}\right)+\frac{-7+8\nu}{4}\cos\left(\frac{\phi}{2}\right)\right); \end{aligned} \tag{63b}$$

where

$$K_{\mathrm{I}}(\theta) = -2\sqrt{2\pi}A_4B_1(\theta), \tag{64a}$$

$$K_{\mathrm{II}}(\theta) = -2\sqrt{2\pi}A_3B_1(\theta). \tag{64b}$$

The stress field in the vicinity of the circular tip of a penny shaped crack inside a body under in-plane extension can be recovered if

$$B_1(\theta) = B_{1\mathrm{s}}(\theta) = \sum_{k=0}^{\infty} D_{2k}\cos(k\theta). \tag{65}$$

Hence, $K_{\mathrm{I}} = K_{\mathrm{Is}}$ and $K_{\mathrm{II}} = K_{\mathrm{IIs}}$ represent symmetric stress intensity factors. If the odd functions are selected from $B_1(\theta)$, it can yield the out-of-plane bending case given by

$$B_1(\theta) = B_{1\mathrm{a}}(\theta) = \sum_{k=1}^{\infty} D_1\sin(k\theta). \tag{66}$$

Here $K_{\mathrm{I}} = K_{\mathrm{Ia}}$ and $K_{\mathrm{II}} = K_{\mathrm{IIa}}$ are anti-symmetric stress intensity factors.

(ii) Penny shaped anticrack or perfectly bonded thin rigid inclusion:

Substitution of Eqs. (53a,b) into Eq. (9) yields the following characteristic equation:

$$\sin(2s\pi) = 0, \tag{67}$$

which yields the minimum root (eigenvalue), contributing to the singular stresses, $s = 1/2$. The singular stress distribution in the vicinity of the circular tip of a penny shaped crack, i.e., $\rho \ll a$, can, therefore, be expressed as follows:

$$\sigma_\rho(\rho,\phi,\theta) = \frac{K_{\mathrm{I}}^{(i)}(\theta)}{\sqrt{2\pi\rho}}\left(\frac{(7-8\nu)}{4}\cos\left(\frac{3\phi}{2}\right)+\frac{5}{4}\cos\left(\frac{\phi}{2}\right)\right) - \frac{K_{\mathrm{II}}^{(i)}(\theta)}{\sqrt{2\pi\rho}}\left(\frac{(5-8\nu)}{4}\sin\left(\frac{3\phi}{2}\right)+\frac{5}{4}\sin\left(\frac{\phi}{2}\right)\right), \tag{68a}$$

$$\sigma_\phi(\rho,\phi,\theta) = \frac{K_{\mathrm{I}}^{(i)}(\theta)}{\sqrt{2\pi\rho}}\left(-\frac{(7-8\nu)}{4}\cos\left(\frac{3\phi}{2}\right)+\frac{3}{4}\cos\left(\frac{\phi}{2}\right)\right) + \frac{K_{\mathrm{II}}^{(i)}(\theta)}{\sqrt{2\pi\rho}}\left(\frac{(5-8\nu)}{4}\sin\left(\frac{3\phi}{2}\right)-\frac{3}{4}\sin\left(\frac{\phi}{2}\right)\right), \tag{68b}$$

$$\tau_{\rho\phi}(\rho,\phi,\theta) = \frac{K_{\mathrm{I}}^{(i)}(\theta)}{\sqrt{2\pi\rho}}\left(-\frac{(5-8\nu)}{4}\cos\left(\frac{3\phi}{2}\right)+\frac{1}{4}\cos\left(\frac{\phi}{2}\right)\right) + \frac{K_{\mathrm{II}}^{(i)}(\theta)}{\sqrt{2\pi\rho}}\left(-\frac{(7-8\nu)}{4}\sin\left(\frac{3\phi}{2}\right)+\frac{1}{4}\sin\left(\frac{\phi}{2}\right)\right), \tag{68c}$$

$$\sigma_\theta(\rho,\phi,\theta) = \frac{2\nu K_{\mathrm{I}}^{(i)}(\theta)}{\sqrt{2\pi\rho}}\cos\left(\frac{\phi}{2}\right) - \frac{2\nu K_{\mathrm{II}}^{(i)}(\theta)}{\sqrt{2\pi\rho}}\sin\left(\frac{\phi}{2}\right) \tag{68d}$$

and

$$U_\rho(\rho,\phi,\theta) = \frac{K_{\mathrm{I}}^{(i)}(\theta)}{G}\sqrt{\frac{\rho}{2\pi}}\left(\frac{(7-8\nu)}{4}\cos\left(\frac{3}{2}\phi\right)+\frac{(5-8\nu)}{4}\cos\left(\frac{\phi}{2}\right)\right) - \frac{K_{\mathrm{II}}^{(i)}(\theta)}{G}\sqrt{\frac{\rho}{2\pi}}\left(\frac{(5-8\nu)}{4}\sin\left(\frac{3\phi}{2}\right)+\frac{(5-8\nu)}{4}\sin\left(\frac{\phi}{2}\right)\right), \tag{69a}$$

$$U_\phi(\rho,\phi,\theta) = -\frac{K_{\mathrm{I}}^{(i)}(\theta)}{G}\sqrt{\frac{\rho}{2\pi}}\left(\frac{(7-8\nu)}{4}\sin\left(\frac{3}{2}\phi\right)+\frac{(7-8\nu)}{4}\sin\left(\frac{\phi}{2}\right)\right) - \frac{K_{\mathrm{II}}^{(i)}(\theta)}{G}\sqrt{\frac{\rho}{2\pi}}\left(\frac{(5-8\nu)}{4}\cos\left(\frac{3\phi}{2}\right)+\frac{(7-8\nu)}{4}\cos\left(\frac{\phi}{2}\right)\right), \tag{69b}$$

where

$$K_j^{(i)}(\theta) = K_{j\mathrm{s}}^{(i)}(\theta) + K_{j\mathrm{a}}^{(i)}(\theta), \quad j = \mathrm{I},\mathrm{II}. \tag{70}$$

In the above equations,

$$K_{\mathrm{I}}^{(i)}(\theta) = -2\sqrt{2\pi}A_4B_1(\theta); \tag{71a}$$

$$K_{\mathrm{II}}^{(i)}(\theta) = -2\sqrt{2\pi}A_3B_1(\theta). \tag{71b}$$

Thus, the stress intensity factors for mode $j = \mathrm{I}, \mathrm{II}$ can be separated into symmetric ($K_{j\mathrm{s}}^{(i)}$, $j = \mathrm{I}, \mathrm{II}$) and anti-symmetric ($K_{j\mathrm{a}}^{(i)}$, $j = \mathrm{I}, \mathrm{II}$) parts in accordance with $B_1(\theta)$ in Eq. (52) assuming $B_{1\mathrm{s}}(\theta)$ and $B_{1\mathrm{a}}(\theta)$, given by Eqs. (65) and (66), respectively.

(iii) Penny shaped thin transversely rigid inclusion (frictionless planar slip permitted):

Substitution of Eqs. (53b) and (54c) into Eq. (10) yields the characteristic equation

$$\cos(2s\pi) = 0. \tag{72}$$

The lowest two roots (eigenvalues) are $s = 1/4$ and $s = 3/4$.

(iv) Penny shaped thin rigid inclusion in part perfectly bonded, the remainder with slip (Fig. 2):

The first two conditions of Eq. (11b) yield the boundary condition

$$\frac{1}{\rho}\frac{\partial U_\rho}{\partial\phi} = 0, \quad \text{at } \theta = \pm\pi. \tag{73}$$

Substitution of Eqs. (53a,b) into Eqs. (11) and (73) yields the characteristic equation

$$\cos(s\pi) = 0, \tag{74}$$

which gives the minimum root $s = 1/2$ for the mode II. The mode II stress intensity factor K_{II} can easily be derived. The singular stress distribution in the vicinity of the front separating the perfectly bonded region to its planar slipping counterpart, can, therefore, be expressed as follows ($\rho \ll a$):

$$\sigma_\rho(\rho,\phi,\theta) = \frac{K_{\mathrm{II}}^{(i)}(\theta)}{\sqrt{2\pi\rho}}\left(\frac{(7-4\nu)}{4}\sin\left(\frac{3\phi}{2}\right)-\frac{5}{4}\sin\left(\frac{\phi}{2}\right)\right), \tag{75a}$$

$$\sigma_\phi(\rho,\phi,\theta) = -\frac{K_{\mathrm{II}}^{(i)}(\theta)}{\sqrt{2\pi\rho}}\left(\frac{(7-4\nu)}{4}\sin\left(\frac{3\phi}{2}\right)+\frac{3}{4}\sin\left(\frac{\phi}{2}\right)\right), \tag{75b}$$

$$\tau_{\rho\phi}(\rho,\phi,\theta) = \frac{K_{\mathrm{II}}^{(i)}(\theta)}{\sqrt{2\pi\rho}}\left(\frac{(7-4\nu)}{4}\cos\left(\frac{3\phi}{2}\right)+\frac{1}{4}\cos\left(\frac{\phi}{2}\right)\right), \tag{75c}$$

$$\sigma_\theta(\rho,\phi,\theta) = -\frac{2\nu K_{\mathrm{II}}^{(i)}(\theta)}{\sqrt{2\pi\rho}}\sin\left(\frac{\phi}{2}\right), \tag{75d}$$

and

$$U_\rho(\rho,\phi,\theta) = \frac{K_{\mathrm{II}}^{(i)}(\theta)}{G}\sqrt{\frac{\rho}{2\pi}}\left(\frac{(7-4\nu)}{4}\sin\left(\frac{3\phi}{2}\right) - \frac{(5-8\nu)}{4}\sin\left(\frac{\phi}{2}\right)\right), \tag{76a}$$

$$U_\phi(\rho,\phi,\theta) = \frac{K_{\mathrm{II}}^{(i)}(\theta)}{G}\sqrt{\frac{\rho}{2\pi}}\left(\frac{(7-4\nu)}{4}\cos\left(\frac{3\phi}{2}\right) - \frac{(7-8\nu)}{4}\cos\left(\frac{\phi}{2}\right)\right), \tag{76b}$$

where $K_{\mathrm{II}}^{(i)}(\theta)$ is defined as in the Case (ii) above.

(v) Penny shaped thin rigid inclusion alongside penny shaped crack:

Substitution of Eqs. (53a,b) and (54b,c) into Eqs. (12a) and (12b), respectively, yields the following characteristic equation:

$$\cos(4s\pi) = \frac{-(8\nu^2 - 12\nu + 5)}{3-4\nu}, \tag{77}$$

which has two pairs of complex roots (eigenvalues) contributing to singular stresses

$$s = s_r + \mathrm{i}s_i, \tag{78}$$

$$\text{(a) } s_r = \frac{1}{4}, \quad s_i = \pm\frac{1}{4\pi}\cosh^{-1}\left(\frac{C^2+1}{2C}\right), \tag{79a}$$

$$\text{(b) } s_r = \frac{3}{4}, \quad s_i = \pm\frac{1}{4\pi}\cosh^{-1}\left(\frac{C^2+1}{2C}\right), \tag{79b}$$

where

$$C = 3 - 4\nu. \tag{80}$$

It may be noted that Eq. (77) is identical to the plane strain version of Eq. (17) for clamped-free case of Williams (1952), obtained by setting $\alpha = 2\pi$, and replacing $\sigma = \nu/(1+\nu)$ by ν.

6. Summary and conclusions

An eigenfunction expansion method is presented to obtain three-dimensional asymptotic stress fields in the vicinity of the front of a penny shaped discontinuity, e.g., crack, anticrack (infinitely rigid lamella), etc., subjected to the far-field torsion (mode III), extension/bending (mode I) and sliding shear/twisting (mode II) loadings. A local orthogonal curvilinear coordinate system (ρ,ϕ,θ), is selected to describe the local deformation behavior in the vicinity of the circular tip of the afore-mentioned penny shaped discontinuity. One of the components of the Euclidean metric tensor, namely g_{33}, is approximated in the derivation of the kinematic relations and the resulting governing system of three partial differential equations. This assumption is consistent with the objective of investigation of the boundary layer effect caused by the presence of a penny shaped crack or anticrack in line with the Griffith–Irwin theory. Because of this approximation, the computed results are valid only in the immediate neighborhood of the circular tip of the penny shaped discontinuity.

Five different discontinuity-surface boundary conditions are considered: (i) penny shaped crack, (ii) penny shaped anticrack or perfectly bonded thin rigid inclusion, (iii) penny shaped thin transversely rigid

inclusion (frictionless planar slip permitted), (iv) penny shaped thin rigid inclusion in part perfectly bonded, the remainder with frictionless slip, and (v) penny shaped thin rigid inclusion alongside penny shaped crack. The computed stress singularity at the tip of a penny shaped crack is identical to its counterpart due to Sack (1946) and Sneddon (1946), who, as mentioned earlier, investigated it under far-field mode I loading condition. This lends confidence to the validity of the procedure employed here.

The circular tip of a penny shaped anticrack (perfectly bonded thin infinitely rigid inclusion) behaves like its crack counterpart as far as the stress singularity is concerned. This explains the initiation of failure from thin rigid inclusions both in the form of highly stiff ceramic platelet reinforcements and embrittlements, such as hydrogen diffused inside a metal lattice or grain boundary. The main difference is, however, that all the stress components at circular tip of an anticrack depend on Poisson's ratio under modes I and II.

In regards to the computed eigenvalues (related to the strength of the stress singularity) and eigenfunction coefficients (related to the stress intensity factors whenever applicable), a penny shaped anticrack (Case (ii)) behaves similar to a corresponding crack in modes I, II, III, and the standard fracture mechanics procedures are applicable here. This is also in agreement with experimentally observed crack initiation and propagation from the regions of platelet reinforcement and HE. In the case of a penny shaped thin transversely rigid inclusion (Case (iii)), the stress singularity in mode I loading is more severe, while mode III behavior is similar to the second case. As regards the case of a penny shaped thin rigid inclusion in part bonded to the matrix, the remainder with frictionless slip (Case (iv)), the mode I crack initiation and propagation from the junction between the bonded and slipping parts of the circular thin rigid inclusion is unlikely, while mode II and mode III cracks are expected to be initiated at this site. In the case of a penny shaped thin rigid inclusion located alongside a crack (Case (v)), the mode I, II eigenvalues are complex, the real parts of which are identical to the corresponding eigenvalues for the Case (iii) discussed above.

Acknowledgements

The author wishes to thank Professor Steele, the editor and two anonymous reviewers for their helpful suggestions on an earlier version of the manuscript.

References

Atkinson, C., 1973. Some ribbon-like inclusion problems. Int. J. Eng. Sci. 11, 243–266.

Brussat, T.R., Westman, R.A., 1974. Interfacial slip around rigid fiber inclusions. J. Compos. Mater. 8, 364–377.

Brussat, T.R., Westman, R.A., 1975. A Westergaard-type stress function for line inclusion problems. Int. J. Solids Struct. 11, 665–667.

Chaudhuri, R.A., Xie, M., 2000. A general eigenfunction expansion solution for three-dimensional crack problems. Compos. Sci. Tech. 60, 2565–2580.

Dundurs, J., Markenscoff, X., 1989. A Green's function formulation of anticracks and their interactions with load induced singularities. ASME J. Appl. Mech. 56, 550–555.

Fung, Y.C., 1965. Foundations of Solid Mechanics. Prentice-Hall, Englewood Cliffs, NJ.

Green, A.E., Zerna, W., 1968. Theoretical Elasticity. Clarendon Press, Oxford, UK.

Hasebe, N., Keer, L.M., Nemat-Nasser, S., 1984. Stress analysis of a kinked crack initiating from a rigid line inclusion. Part I: Formulation. Mech. Mater. 3, 131–145.

Hertzberg, R.W., 1996. Deformation and Fracture Mechanics of Engineering Materials, fourth ed. John Wiley & Sons, Inc., Chapter 11.

Korn, G.A., Korn, T.M., 1968. Differential Geometry, Mathematical Handbook, second ed. McGraw-Hill, New York, Chapter 17.

Sack, R.A., 1946. Extension of Griffith theory of rupture to three dimensions. Proc. Phys. Soc. Lond. 58, 729–736.

Sih, G., 1965. Plane extension of rigidly embedded line inclusions. In: Huang, T.C., Johnson, M.W. (Eds.), Developments in Mechanics. Wiley, New York, pp. 361–367.

Sneddon, I.N., 1946. The distribution of stress in the neighborhood of a crack in an elastic solid. Proc. Royal Soc. Lond., Ser. A 187, 229–260.

Williams, M.L., 1952. Stress singularities resulting from various boundary conditions in angular corners of plates in extension. ASME J. Appl. Mech. 19, 526–528.

Williams, M.L., 1957. On the stress distribution at the base of a stationary crack. ASME J. Appl. Mech. 24, 109–114.

Xie, M., Chaudhuri, R.A., 1998. Three-dimensional stress singularity at a bimaterial interface crack front. Compos. Struct. 40, 137–147.